Coherent diffractive imaging and partial coherence

Garth J. Williams,[1] Harry M. Quiney,[1] Andrew G. Peele,[2] and Keith A. Nugent[1]
[1]*School of Physics, The University of Melbourne, Victoria 3010, Australia*
[2]*Department of Physics, La Trobe University, Bundoora, Victoria 3086, Australia*
(Received 18 September 2006; revised manuscript received 20 November 2006; published 6 March 2007)

We formulate coherent diffractive imaging in the framework of partially spatially coherent diffraction. We find that the reconstruction can be critically dependent on the degree of coherence in the illuminating field and that even a small departure from full coherence may invalidate the conventional assumption that a mapping exists between an exit surface wave of finite support and a far field diffraction pattern. We demonstrate that the introduction of sufficient phase curvature in the illumination can overcome the adverse effects of partial coherence.

DOI: 10.1103/PhysRevB.75.104102 PACS number(s): 61.10.Nz, 07.85.Qe, 42.30.Rx, 87.59.−e

I. INTRODUCTION

Protein crystallography relies on the diffraction of x rays from protein crystals and is therefore highly dependent on the capacity to make such crystals. Unfortunately, many proteins will not form the three-dimensional crystals required, and so attention is turning to the possibility of acquiring structures from noncrystalline diffraction using the emerging free-electron laser sources.[1] This is now an active area for research.

This approach to imaging was proposed many years ago by Sayre.[2] The mathematical possibility of obtaining an almost unique reconstruction was analyzed by Bates,[3] an analysis that was extended and discussed by Miao at *et al.*[4] The method for reconstruction is an iterative approach in which an object is found that obeys known size constraints applied in real space and predicts the correct measured intensity in reciprocal space, an approach based on work in electron microscopy published over 30 years ago[5] but with algorithms that have been improved over the intervening years.[6,7] The method was experimentally demonstrated by Miao *et al.*[8] in 1999 and, since then, a number of additional experimental works have been published, including some very striking images of yeast cells,[9] nanocrystals,[10] and a three-dimensional reconstruction of a manufactured gold object.[11]

Much of the thinking in this area has its genesis in crystallography, a field that rests on two major assumptions: the diffracting object is periodic and the incident wave can be considered planar over the scale of a unit cell. Coherent diffractive imaging has relaxed the first of these assumptions, and recent work has shown that it is also possible to relax the second. Modern x-ray optics can produce an x-ray focus on the order of 15 nm across,[12] a figure that is comparable to the size of a large protein. It is therefore possible to illuminate even single molecules with a wave front with significant curvature. In this case, the reconstruction is truly unique.[13] The ability to perform such a reconstruction requires a very good characterization of the illuminating field, a possibility that has been demonstrated,[14] and it has been shown that it is possible to use this information to reconstruct a diffracting object.[15]

While, in the longer term, the free-electron laser will offer an extremely high degree of spatial coherence, current state-of-the-art experiments use third-generation synchrotron sources that have a much smaller coherent fraction. The role of coherence in coherent diffraction imaging has been discussed rather qualitatively elsewhere,[16] and this study concluded that the coherence length must be at least twice the size of the object in order to properly encode the information.

The aim of this paper is to frame a partially coherent theory of diffraction by non-periodic samples to explore the role of coherence and to understand how it can be controlled. We develop and test a theory that encompasses both planar and curved incident fields and find, for plane-wave illumination, that the coherence requirements for reliable imaging are rather more restrictive than previously thought.

Section II develops a model for the partially coherent illuminating field that allows the comparison of illumination that is either curved or planar, but for which the coherence length is identical. Section III reviews the standard formalism for far-field partially coherent diffraction. Section IV applies the methodology of far-field diffraction for both curved and planar illumination and demonstrates the interplay between the effects of coherence and phase curvatures. Section V tests the conclusions of Sec. IV using simulations, and the conclusions are discussed in Sec. VI

II. THE ILLUMINATION OF THE SAMPLE

Consider the experimental conditions shown in Fig. 1. Figure 1(a) shows the conventional coherent diffractive imaging configuration in which a plane wave is incident on a sample and the scattered intensity is measured in the far field. Figure 1(b) shows a comparable experiment in which a lens that produces a curved wave field is introduced. The sample in this case is placed at the point at which the beam has reexpanded to the radius it had immediately before the lens. Assuming that the lens is perfectly efficient and focuses all of the incident light, then the field at the sample has the same intensity as that entering the lens. We show below that it will also have the same coherence length.

We assume that a lens is placed at $z=0$ and uses a three-dimensional coordinate system $(\boldsymbol{r},z)$, where $\boldsymbol{r}=(x,y)$ is a two-dimensional vector in a plane normal to the optical axis and at a location z along it (Fig. 2) and describes the field at

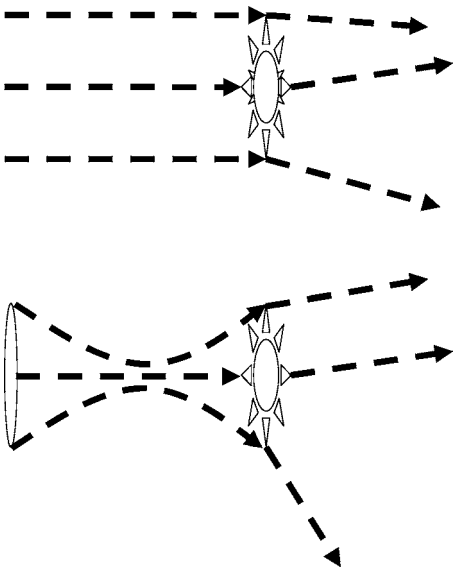

FIG. 1. Schematic of the two illumination conditions considered. Assuming an ideal perfect lens, both have identical intensities and coherence lengths at the sample plane. However, the illumination with a lens has an additional phase curvature given by the focal length of the lens.

the plane z using the mutual optical intensity $J_z(\boldsymbol{r}_1,\boldsymbol{r}_2)$. We model the field entering the lens using the generalized Schell model[17] for the mutual optical intensity (MOI),

$$J_0(\boldsymbol{r}_1,\boldsymbol{r}_2) = \psi(\boldsymbol{r}_1)\psi^*(\boldsymbol{r}_2)g(\boldsymbol{r}_1-\boldsymbol{r}_2). \tag{1}$$

The coherence length of the light is specified by the characteristic width of the coherence factor $g(\boldsymbol{x})$, and we assume that the field is quasimonochromatic and is described with a wave number $k_0=2\pi/\lambda$. In the case of an incoherent source, $s(\boldsymbol{r}_s)$, at some distance, z, from the plane of interest, we have the special case where

$$\psi(\boldsymbol{r}) = \frac{i}{\lambda z}\exp\left(ik_0\frac{r^2}{\lambda z}\right) \tag{2}$$

and

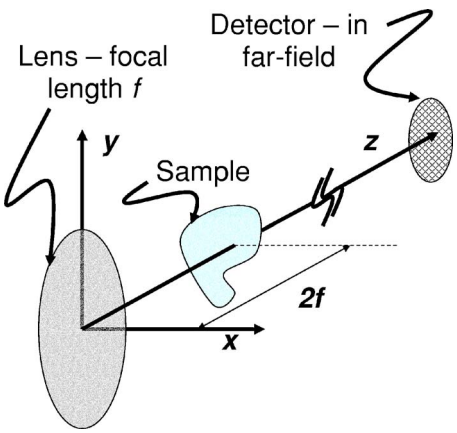

FIG. 2. (Color online) Schematic of the experimental system being modeled and the coordinate system used.

$$g(\boldsymbol{r}_1-\boldsymbol{r}_2) = \left(\frac{k_0}{2\pi}\right)^2\int s(\boldsymbol{r}_s)\exp[-ik_0(\boldsymbol{r}_1-\boldsymbol{r}_2)\cdot\boldsymbol{r}_s]d\boldsymbol{r}_s, \tag{3}$$

which is the van Cittert-Zernike theorem. Physically, this is a set of mutually incoherent spherical waves with an angular distribution determined by the physical shape of the source. Equation (1) generalizes this description to allow for an incoherent superposition of arbitrary waves and so allows for the possibility of propagation through an optical system or other refracting or reflecting medium.

As a good physical model for the radiation field, one can regard $g(\boldsymbol{x})$ as the Fourier transform of an incoherent source distribution viewed through an optical system that transfers a point radiator in the source plane (that is, Green's function for the optical system) into a wave described by $\psi(\boldsymbol{r})$. In free space, then, $\psi(\boldsymbol{r})$ becomes a spherical wave, and we recover the van Cittert-Zernike theorem.

We suppose that this passes through a thin lens with focal length f, resulting in the MOI leaving the lens described by[18]

$$J_{0^+}(\boldsymbol{r}_1,\boldsymbol{r}_2) = \psi(\boldsymbol{r}_1)\psi^*(\boldsymbol{r}_2)\exp\left(-ik_0\frac{\boldsymbol{r}_1^2-\boldsymbol{r}_2^2}{2f}\right)g(\boldsymbol{r}_1-\boldsymbol{r}_2). \tag{4}$$

For simplicity, we assume that the incident wave components are planar with uniform amplitude A_0,

$$\psi(\boldsymbol{r}) = A_0, \tag{5}$$

and we write the coherence factor in terms of a coherence length

$$g(\boldsymbol{r}_1-\boldsymbol{r}_2) = \exp\left(-\frac{|\boldsymbol{r}_1-\boldsymbol{r}_2|^2}{2\ell_c^2}\right), \tag{6}$$

giving

$$J_{0^+}(\boldsymbol{r}_1,\boldsymbol{r}_2) = A_0^2\exp\left[-\left(\frac{\boldsymbol{r}_1-\boldsymbol{r}_2}{2\ell_c^2}+ik_0\frac{\boldsymbol{r}_1+\boldsymbol{r}_2}{2f}\right)\cdot(\boldsymbol{r}_1-\boldsymbol{r}_2)\right]. \tag{7}$$

We now propagate this to an arbitrary distance z from the lens using the standard paraxial partially coherent propagation rules to obtain

$$J_z(\boldsymbol{r}_1,\boldsymbol{r}_2) = A^2(z)\exp\left\{-\left[\frac{\boldsymbol{r}_1-\boldsymbol{r}_2}{2\ell_c^2(z)}+ik_0\frac{\boldsymbol{r}_1+\boldsymbol{r}_2}{2R(z)}\right]\cdot(\boldsymbol{r}_1-\boldsymbol{r}_2)\right\}, \tag{8}$$

where

$$\ell_c(z) = \left|\frac{f-z}{f}\right|\ell_c,$$

$$R(z) = f-z,$$

$$A^2(z) = \left(\frac{f}{f-z}\right)^2 A_0^2. \tag{9}$$

Note that the coherence length in the radiation is position dependent, becoming zero at the (perfect) focus as the beam collapses and then increasing again. The collapse of the co-

herence length at the focus is a nonphysical artifact of our assumption of a perfect, infinite lens. However, the coherence length returns to its value at the entrance of the lens at the position $z_s=2f$, and so we use this point to compare the curved beam illumination with that in which the component waves are planar, as described by Eq. (5). In our model, the scattering object is placed at a significant distance (one focal length) from the focus, and so the field at this point will be described as a Fresnel diffraction pattern of the lens pupil and will be free of the intensity zeroes and rapid amplitude inhomogeneities that characterize a field close to a focal point.

We note that the assumption of a lens with infinite extent leads to Eq. (7), having singular behavior at the focus. In the real case of a finite lens, the singular behavior disappears but the amplitude at the sample plane is modified by diffraction from the lens pupil. For the purposes of the present discussion, then, we will retain the assumption of an infinite lens so as to obviate the complications arising from amplitude modulations in the diverging illumination.

Under the infinite lens approximation, the MOI at the chosen sample plane has the form

$$J_{z_s}(\boldsymbol{r}_1,\boldsymbol{r}_2) = A_0^2 \exp\left[-\left(\frac{\boldsymbol{r}_1-\boldsymbol{r}_2}{2\ell_c^2} - ik_0\frac{\boldsymbol{r}_1+\boldsymbol{r}_2}{2f}\right)\cdot(\boldsymbol{r}_1-\boldsymbol{r}_2)\right]. \tag{10}$$

Thus, the wave at the sample plane has the same coherence length and magnitude as the wave entering the lens, but has a phase curvature associated with the focal length of the lens (Fig. 1). We note that in the electron microscopy community, this illumination condition would be described as having a "focusing error" of f, and that the intensity distribution in the sample illumination will be described by the Fresnel diffraction pattern of the lens pupil (that is, ignoring the focusing effect of the lens) at a distance of f from the pupil. To a very good approximation, then, the illumination will be identical to the distribution at the pupil plane, a statement that is strictly true for the limit of a very large pupil.

The planar component wave limit [Eq. (5)] can be recovered by taking the limit $f\to\infty$ so that

$$J_{z_s}(\boldsymbol{r}_1,\boldsymbol{r}_2) \to A_0^2 \exp\left(-\frac{|\boldsymbol{r}_1-\boldsymbol{r}_2|^2}{2\ell_c^2}\right). \tag{11}$$

III. PARTIALLY COHERENT FAR-FIELD DIFFRACTION

Let us assume that the scattering structure is thin and has a complex transmission described by $\sigma(\boldsymbol{r})$. We illuminate it with a field described by $J_{z_s}(\boldsymbol{r}_1,\boldsymbol{r}_2)$. The field leaving the sample, $J^{sc}_{z_s}(\boldsymbol{r}_1,\boldsymbol{r}_2)$, has the form

$$J^{sc}_{z_s}(\boldsymbol{r}_1,\boldsymbol{r}_2) = J_{z_s}(\boldsymbol{r}_1,\boldsymbol{r}_2)\sigma(\boldsymbol{r}_1)\sigma^*(\boldsymbol{r}_2). \tag{12}$$

In coherent diffractive imaging, we are concerned with imaging very small objects and so can safely assume that all observations are made in the far field. In this limit, the distance between a point in the scattering object and a point in the detector plane R can be approximated by

$$R \sim r - \boldsymbol{s}\cdot\boldsymbol{r}, \tag{13}$$

where $r\equiv|\boldsymbol{r}|$, $r_1\equiv|\boldsymbol{r}_1|$, and $r_2\equiv|\boldsymbol{r}_2|$ and $\boldsymbol{s}_1$ and $\boldsymbol{s}_2$ describe the unit vectors pointing at the field points in the detector plane. In this limit, the mutual optical intensity function in the far field can be written in terms of the scattered field as[19]

$$J_\infty(\boldsymbol{s}_1 r_1,\boldsymbol{s}_2 r_2) = \frac{\exp[ik(r_1-r_2)]}{r_1 r_2}\int\int J^{sc}_{z_s}(\boldsymbol{r}_1,\boldsymbol{r}_2) \times\exp[-ik_0(\boldsymbol{s}_2\cdot\boldsymbol{r}_2-\boldsymbol{s}_1\cdot\boldsymbol{r}_1)]d\boldsymbol{r}_1 d\boldsymbol{r}_2. \tag{14}$$

For simplicity, we write

$$J^{sc}_\infty(r_1\boldsymbol{s}_1,r_2\boldsymbol{s}_2) = L^{sc}(\boldsymbol{s}_1,\boldsymbol{s}_2)\frac{\exp[ik(r_1-r_2)]}{r_1 r_2},$$

where

$$L^{sc}(\boldsymbol{s}_1,\boldsymbol{s}_2) \equiv \int\int J^{sc}_{z_s}(\boldsymbol{r}_1,\boldsymbol{r}_2)\exp[-ik_0(\boldsymbol{s}_2\cdot\boldsymbol{r}_2-\boldsymbol{s}_1\cdot\boldsymbol{r}_1)]d\boldsymbol{r}_1 d\boldsymbol{r}_2. \tag{15}$$

We change the variables

$$\boldsymbol{r}\equiv\boldsymbol{r}_1, \quad \boldsymbol{x}\equiv\boldsymbol{r}_2-\boldsymbol{r}_1, \tag{16}$$

$$\boldsymbol{s}\equiv\boldsymbol{s}_1, \quad \zeta\equiv\boldsymbol{s}_2-\boldsymbol{s}_1, \tag{17}$$

so that

$$L^{sc}(\boldsymbol{s},\boldsymbol{s}+\zeta) = \int\int J^{sc}_{z_s}(\boldsymbol{r},\boldsymbol{r}+\boldsymbol{x})\exp\{-ik_0[(\zeta+\boldsymbol{s})\cdot\boldsymbol{x} + \zeta\cdot\boldsymbol{r}]\}d\boldsymbol{r}d\boldsymbol{x} \tag{18}$$

and, ignoring constant corresponding to the factor in front of the integral in Eq. (14), we shall write the far-field scattered intensity as $I^{sc}_\infty(\boldsymbol{s})=L(\boldsymbol{s},\boldsymbol{s})$. Thus, the measured far-field intensity has the form

$$I^{sc}_\infty(\boldsymbol{s}) = \int J^{sc}_{z_s}(\boldsymbol{r},\boldsymbol{r}+\boldsymbol{x})\exp(-ik_0\boldsymbol{s}\cdot\boldsymbol{x})d\boldsymbol{x}d\boldsymbol{r}. \tag{19}$$

This is a rather general expression for the diffractive imaging problem in which one wishes to invert Eq. (19) to recover the scattering function from the intensity measurement. *Coherent* diffractive imaging is typically concerned with the inversion of this equation for a scattering object of known and finite extent in the limit

$$A(\boldsymbol{r}) \to A_0,$$

$$g(\boldsymbol{x}) \to 1, \tag{20}$$

where A_0 is the uniform amplitude of an incident coherent plane wave.

In this work, we wish to draw a distinction between *far-field* diffraction [defined in Eq. (13)] and *Fraunhofer* diffraction, which makes the additional assumption, given in Eq. (20), that the incident field is planar. Some recent work has relaxed the assumption of a uniform plane wave and has shown that there are some advantages to incorporating phase curvature in the incident light. It has been shown that the

Fraunhofer assumption leads to a coherent diffractive imaging regime in which the phase recovery is almost unique. The Fresnel regime, which includes far-field, but not Fraunhofer, diffraction has been shown to have a unique solution and to provide for better convergence.

The primary objective of this paper is to explore the consequences of the relaxation for the second assumption in Eq. (20), i.e., the assumption of perfect coherence. This will be done in two parts. The first will explore partially coherent diffraction in the Fraunhofer limit. The second will consider the more general case of partially coherent spherically curved incident wave fronts.

IV. THE SCATTERED FIELD AND THE MEASUREMENT PROCESS

A. Illumination by curved component waves

We now use the illumination described by Eq. (10) to illuminate a diffracting sample using Eq. (12) and put this result into the expression for the far-field intensity [Eq. (19)] to obtain an expression for the far-field intensity of a thin object illuminated by partially coherent diverging light,

$$I_{\infty}^{sc}(\boldsymbol{s}) = A_0^2 \int \sigma(\boldsymbol{r})\sigma^*(\boldsymbol{r}+\boldsymbol{x})\exp\left(-ik_0\frac{\boldsymbol{r}\cdot\boldsymbol{x}}{f}\right)d\boldsymbol{r} \times \exp(-\mu|\boldsymbol{x}|^2)\exp(-ik_0\boldsymbol{s}\cdot\boldsymbol{x})d\boldsymbol{x}, \tag{21}$$

where

$$\mu \equiv \frac{1}{2\ell_c^2} + \frac{ik_0}{f}. \tag{22}$$

The plane-wave case is the limit $f \to \infty$ and the coherent case is the limit $\ell_c \to \infty$. The conventional paradigm for coherent diffraction imaging is where both these limits pertain.

B. Illumination by planar component waves

In the model adopted here, planar illumination is described by taking the limit $f \to \infty$ in Eq. (21), yielding an expression for the measured intensity for a planar partially coherent field,

$$I_{\infty}^{sc}(\boldsymbol{s}) = A_0^2 \int\int \sigma(\boldsymbol{r})\sigma^*(\boldsymbol{r}+\boldsymbol{x})d\boldsymbol{r}\exp\left(-ik_0\boldsymbol{s}\cdot\boldsymbol{x} - \frac{|\boldsymbol{x}|^2}{2\ell_c^2}\right)d\boldsymbol{x}. \tag{23}$$

In the coherent limit, $\ell_c \to \infty$, we obviously recover the conventional result that the intensity distribution is the Fourier transform of the autocorrelation function of the scattering distribution.

Note that Eq. (23) is essentially a convolution integral over the diffracted field, and so the observable effect of partial coherence is to convolve the coherent diffraction pattern with the Fourier transform of $g(\boldsymbol{x})$.[20] This effect has also been predicted and observed by other workers.[21] It is easy to show that any real zeroes present in the coherent diffraction pattern are eliminated by the convolution described above. This mechanism therefore eliminates the asymptotic distribution of zeroes that ensures the finite support of the object. There can therefore be no function of finite support that is consistent with the measured partially coherent diffraction pattern.[22] A small departure from full coherence is consequently sufficient to formally render $\sigma(\boldsymbol{r})$ irretrievable from its diffraction data using any conventional iterative method based on coherent propagation.

C. Discussion

As discussed above, formally, the slightest deviation from perfect coherence means that a solution consistent with the data and with a finite support does not exist. The precise combination of parameters for which a practical breakdown occurs in the consistency between finite support and measured intensity depends on many factors, and is difficult to quantify in general. However, a great deal of sensitivity is to be expected to the coherence of the illumination, far greater than is implied by a simple requirement that the coherence length should encompass the autocorrelation of the object.[16]

The addition of spherical illumination changes the character of the reconstruction, as we now discuss. Note that $\exp[-\mu|\boldsymbol{x}|^2]$ is the product of an oscillatory term from the spherical illumination and an exponentially decaying term from the partial coherence. If f is sufficiently small, the imaginary part of μ will cause this exponential term to oscillate so rapidly that only regions close to $|\boldsymbol{x}|=0$ can contribute to the integrand. The measured intensities then approach the fully coherent limit and, in this case, the methods of coherent diffractive imaging should yield a good result, subject to the usual qualifications of stagnation of the iterative procedure and the deleterious effects of the reconstruction of noise and other experimental practicalities.

The condition for this to hold is that $\frac{k_0\ell_c^2}{f} \gg \pi$ so that

$$f \ll \frac{2\ell_c^2}{\lambda}. \tag{24}$$

For typical x-ray experiments, where $\lambda \approx 1$ nm and $\ell_c \approx 10$ μm, then we require $f \ll 20$ cm. This is easily achieved experimentally and is obeyed by the recently reported experiments using spherical beam coherent diffraction. It is interesting to note that the conditions where the effects of coherence are important apply precisely to the regime of the modern third-generation synchrotron source.

V. SIMULATIONS

Utilizing the framework developed in Sec. IV, we used a test object (Fig. 3) to simulate the far-field intensity that would arise in the detector from various values of the coherence length and curvature of the incident illumination. The convergence behavior and fidelity of the reconstruction to the original object were then studied as a function of these parameters.

The partially coherent intensity at the detector was calculated by performing a fast Fourier transform (FFT) on the object and squaring the resultant complex simulated wave amplitude to arrive at an intensity measurement. The effects of partial coherence were then incorporated by convolving the coherent intensity with a Gaussian of width determined

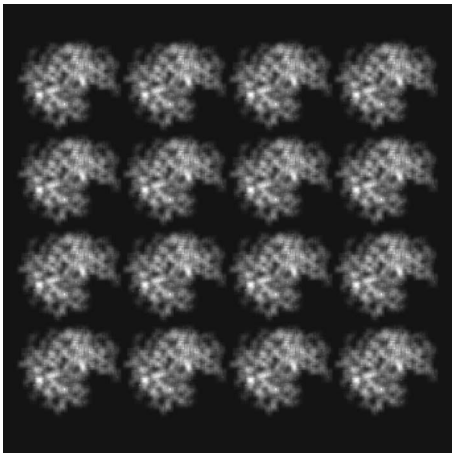

FIG. 3. The test object used in the simulations. The object spanned 320×288 pixels of the 900×900 pixel FFT arrays and was composed of 16 identical constituent subunits. The object was real and positive.

by the coherence length, as described by either Eq. (21) or (23). In the plane of the sample, the magnitude of the illumination was uniform and constant over all fits, and the phase was assumed spherical with some radius of curvature R: $\exp(ik_0r^2/R)$.

We present here the analysis of the resultant reconstructions for 36 simulated intensities: 12 different coherence lengths at three different curvatures. The iterative fitting was accomplished by means of a combination of error reduction (ER) and hybrid input/output (HIO) algorithms. Our recipe was 150 cycles of ER, 40 HIO with $\beta=0.9$, 150 ER, 50 HIO with $\beta=0.95$, and 150 ER. No less than ten sets of random starting phases were used per trial. The support constraint was taken as a square of side of 320 pixels, just larger than the gross size of the object, i.e., 288×320. The FFT array was 900×900 pixels. The curvatures were such that the phase varied from the center to a corner of the object by 2π at low curvature ($N_F=2$), 5π at intermediate curvature ($N_F=5$), and 8π at high curvature ($N_F=8$), where N_F is the so-called Fresnel number. During the fitting, the progress was monitored by means of the usual metric

$$\chi^2 = \frac{\sum_i (F_i - \sqrt{I_i})^2}{\sum_i I_i^2}, \tag{25}$$

where F_i is the calculated Fourier magnitude of the estimate and I_i is the simulated partially coherent diffraction pattern in pixel i. We will also use metrics with the form of Eq. (25) to compare the final iterate to the original object.

In Fig. 4, we plot the mean χ^2 with uncertainty given by the standard deviation of the collection of all fits for different combinations of incident curvature and coherence length. We normalize the coherence length to the largest dimension of the test object, Γ, for simplicity. It is interesting to note that when the coherence is poor and the incident wave is only slightly curved, ER finds multiple differing reconstructions

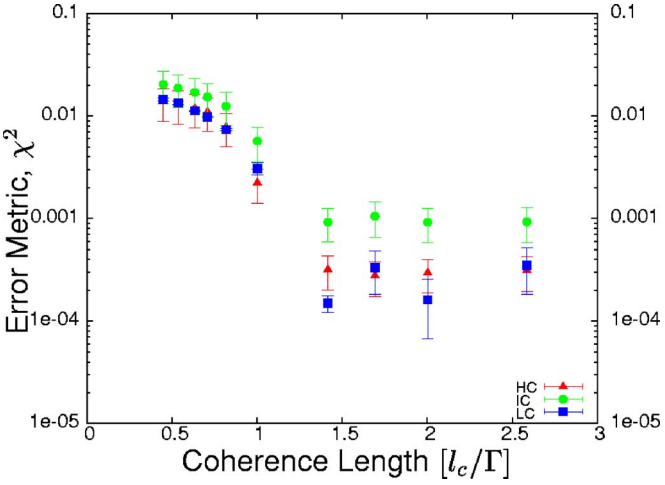

FIG. 4. (Color online) Mean—with uncertainty given by the standard deviation—of the error metric for each fit plotted against the coherence length of the illumination at the sample, normalized to the largest object dimension Γ. It is interesting to note that in the case of low curvature, $N_F=2$, the standard deviation becomes small at short coherence lengths.

that match the simulated data equally well; this phenomenon disappears as the curvature increases.

A measure of agreement between the best results, as judged by Eq. (25), and the original object against curvature is shown in Fig. 5. The former is derived from Eq. (25) and stated

$$\xi = 1 - \sqrt{\sum_i (f_i - f_i^t)^2 \Big/ \sum_i I_i}, \tag{26}$$

where f_i is the best estimate and f_i^t is the truth object in pixel i. A large ξ will indicate good agreement with the object. In Fig. 5, we display the average value of ξ over six values of the coherence length: 1.4, 1.7, 2.0, 2.6, 4.5, and 140 times the size of the object. It is clear that as the curvature is increased in the presence of imperfect coherence, the quality of the reconstruction improves.

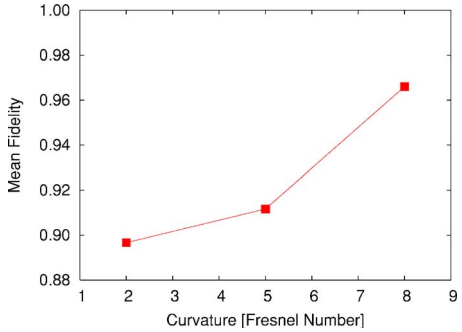

FIG. 5. (Color online) Mean fidelity over six simulations where the coherence length exceeds the sample size against the three curvatures of the illumination discussed in the text. The average fidelity is low for low curvature in the incident illumination and increases as the curvature increases, showing that as curvature is increased the deleterious effects of partial coherence are reduced.

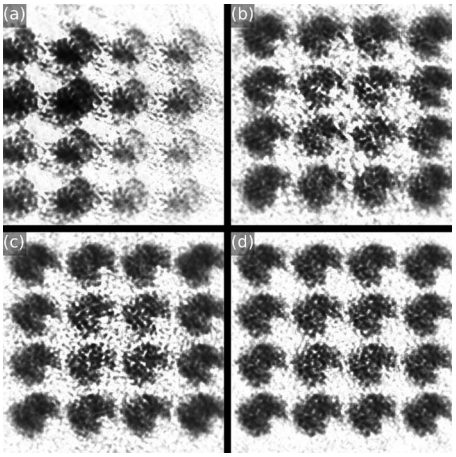

FIG. 6. The reconstructed object when the simulated illumination had a coherence length of 71% the object size. Figure 4(a) is the case of plane-wave illumination where the reconstruction clearly fails. Figures 4(b) and 4(c)—the cases of $N_F=2$ and $N_F=5$, respectively—show considerable improvement, while the highest curvature case, $N_F=8$, is nearly correct. The images are scaled identically on a contrast-enhanced grayscale map.

In Fig. 6, we present the results of simulations where the coherence length is only 71% of the object size. The reconstructions are presented in the support used during iterative phase retrieval. The images have been identically scaled and contrast enhanced to highlight the behavior. It is clear that the plane wave case [Fig. 4(a)] has failed with this level of coherence. Even the low curvature case [Fig. 4(b)] shows a marked improvement. We note that the addition of curvature to the simulation has forced the localization of the object in the array. As the curvature is increased to $N_F=5$ [Fig. 4(c)] and finally $N_F=8$ [Fig. 4(d)], the improvement is marked, with the highest curvature case giving a very good estimate.

VI. DISCUSSION AND CONCLUSIONS

The observation that the convergence of conventional iterative schemes is strikingly dependent on having an extremely high degree of coherence is remarkable. In Sec. IV, we noted the need for a well-defined distribution of asymptotic zeroes to enable an object to be both consistent with the data and consistent with the known support. In this ideal limit, partially coherent data will therefore be precluded from ever being able to be properly reconstructed. We note that this observation is consistent with the report that experiments with fully coherent visible data always show very good convergence properties[23]—optical lasers are, for all practical purposes, perfectly coherent. Moreover, we found that, in the presence of partial coherence, the converged reconstruction often displayed only a poor relationship to the diffracting object.

The theoretical development indicated that phase curvature introduces an additional factor that ameliorates the impact of partial coherence. In addition, the use of Fresnel diffraction patterns show significantly better convergence properties and a unique solution in the fully coherent limit, and so data of this form would in any case be more robust to partial coherence. Our simulations showed that partially coherent diffraction from curved x-ray beams was indeed significantly more likely to converge on a valid solution.

We note in conclusion that the iterative methods used to solve these assume a Fourier transform relationship between the field leaving the object and the field in the detector plane. That is, perfect coherence is a central assumption underlying the technique. Therefore, the lack of convergence in the presence of partial coherence is, perhaps, not surprising. We suggest that if coherent diffractive imaging is to become a reliable technique at modern synchrotron sources, then there is a need to develop solution methods that do not have a built-in assumption of coherence and can properly model the experimental system.

ACKNOWLEDGMENTS

The authors acknowledge support from the Australian Research Council Centre of Excellence and Fellowship Programs.

[1] R. Neutze, R. Wouts, D. Van Der Spoel, E. Weckert, and J. Hajdu, Nature (London) **406**, 752 (2000).
[2] D. Sayre, Acta Crystallogr. **5**, 843 (1952).
[3] R. H. T. Bates, Optik (Jena) **61**, 247 (1982).
[4] J. Miao, D. Sayre, and H. N. Chapman, J. Opt. Soc. Am. A **15**, 1662 (1998).
[5] R. W. Gerchberg and W. O. Saxton, Optik (Jena) **35**, 237 (1972).
[6] J. R. Fienup, Appl. Opt. **21**, 2758 (1982).
[7] V. Elser, J. Opt. Soc. Am. A **20**, 40 (2003).
[8] J. W. Miao, P. Charalambous, J. Kirz, and D. Sayre, Nature (London) **400**, 342 (1999).
[9] P. Thibault, V. Elser, C. Jacobsen, D. Shapiro, and D. Sayre, Acta Crystallogr., Sect. A: Found. Crystallogr. **62**, 248 (2006).
[10] G. J. Williams, M. A. Pfeifer, I. A. Vartanyants, and I. K. Robinson, Phys. Rev. Lett. **90**, 175501 (2003).
[11] H. N. Chapman, A. Barty, S. Marchesini, A. Noy, S. R. Haue-Riege, C. Cui, M. R. Howells, R. Rosen, H. He, J. C. H. Spence, U. Weierstall, T. Beetz, C. Jacobsen, and D. Shapiro, J. Opt. Soc. Am. A **23**, 1179 (2006).
[12] W. L. Chao, B. D. Harteneck, J. A. Liddle, E. H. Anderson, and D. T. Attwood, Nature (London) **435**, 1210 (2005).
[13] T. A. Pitts and J. F. Greenleaf, IEEE Trans. Ultrason. Ferroelectr. Freq. Control **50**, 1035 (2003).
[14] H. M. Quiney, A. G. Peele, Z. Cai, D. Paterson, and K. A. Nugent, Nat. Phys. **2**, 101 (2006).
[15] G. J. Williams, H. M. Quiney, B. B. Dhal, C. G. Tran, K. A. Nugent, A. G. Peele, D. Paterson, and M. D. de Jonge, Phys. Rev. Lett. **97**, 025506 (2006).
[16] J. C. H. Spence, U. Weierstall, and M. Howells, Ultramicroscopy **101**, 149 (2004).

[17] K. A. Nugent, J. Opt. Soc. Am. A **8**, 1574 (1991).
[18] A. S. Marathay, *Elements of Optical Coherence Theory* (Wiley, New York, 1982), pp. 182–185.
[19] L. Mandel and E. Wolf, *Optical Coherence and Quantum Optics* (Cambridge University Press, Cambridge, 1995), pp. 229–231.
[20] J. J. A. Lin, D. Paterson, A. G. Peele, P. J. McMahon, C. T. Chantler, K. A. Nugent, B. Lai, N. Moldovan, Z. Cai, D. C. Mancini, and I. McNulty, Phys. Rev. Lett. **90**, 074801 (2003).
[21] I. A. Vartanyants and I. K. Robinson, J. Phys.: Condens. Matter **13**, 10593 (2001).
[22] R. G. Walker, Opt. Acta **28**, 735 (1981).
[23] J. C. H. Spence, U. Weierstall, and M. Howells, Philos. Trans. R. Soc. London, Ser. A **360**, 875 (2002).